ANALYSIS OF ROLLING CONTACT FATIGUE AND FRACTURE

G. T. Hahn, V. Bhargava, H. Yoshimura and C. Rubin

Department of Mechanical and Materials Engineering, Vanderbilt University, Nashville, TN 37235, USA

ABSTRACT

This paper examines the fatigue and fracture of rims subjected to repeated rolling contact, in other words, the processes responsible for the spalling and shelling of bearings, wheels, rails, gears, cams, etc. It touches on (1) contact stresses and strains, (2) crack initiation, (3) the predominantly Mode II cyclic crack growth driving force, and (4) crack growth rate, ΔK_{II}-da/dN, measurements. The contributions of cyclic hardening and softening, the hydrostatic pressure, and the crack face friction are discussed. Finally, the extent to which a rim life prediction can be extracted from the fracture mechanics analysis is tested.

KEYWORDS

Rolling contact failure; spalling; shelling; rolling contact fatigue; rim life; contact stresses; Mode II cyclic crack growth; ΔK_{II}; crack face friction.

INTRODUCTION

Repeated rolling contact can lead to the fatigue and fracture of a rim. Unlike wear processes, which operate within ~ 10μm from the contact surface and produce tiny flakes, fatigue and fracture can proceed at depths of the order of millimeters and produce proportionately bigger fragments, spalling and shelling (Syniuto and Corrow, 1970; Sugino et al., 1971; Martin and Hay, 1972; Kunikake et al., 1970). Statistics published by Hengel (1978) reveal that the fracture (shelling) of freight car wheels is a multi-million-dollar-per-year problem in its own right. To this must be added the cost of premature failures of rails, bearings, gears, cams, etc. There is evidence that rolling contact proceeds by the cyclic growth of cracks or cracks that are initiated during rolling (Lundberg and Palmgren, 1947). An analysis of rim life must involve 5 elements of the problem:

(i) Contact Stresses and Strains. The crack initiation process and the cyclic crack growth driving force depend on the contact stress and strain fluctuations produced by repeated rolling contacts.

(ii) Constitutive Relations for Cyclic Flow. The peak contact stress and strain fluctuations, in turn, are influenced by the cyclic hardening and cyclic softening of the rim material. This depends on the constitutive relations of the rim material and the character of the non-reversing, small plastic strain amplitude cycles peculiar to repeated rolling contact.

(iii) Initiating Defect. Cyclic crack growth and rim life depend on either the size and geometry of the pre-existing crack or on the duration and product of the initiation process that converts a microstructural discontinuity into a crack.

(iv) Driving Force for Cyclic Crack Growth. The predominantly Mode II ΔK-driving force for cyclic crack growth depends on items (i)-(iii) and on the crack face friction.

(v) Cyclic Crack Growth Rate. The cyclic crack growth rate depends on the ΔK_{II}-driving force and the ΔK_{II}-da/dN relation which is a measurable material property.

Insights into improved material performance require an appreciation of the relative contributions of items (ii), (iii) and (v), and their sensitivity to alloying and processing. While a great deal of empirical information has accumulated (Hoo, 1981), the present grasp of rim life, and the potential for improved rim performance in terms of the 5 basic elements of the problem, is still limited. The very preliminary test of fracture mechanics predictions of rim life, presented in the last section of this paper suggests that meaningful predictive capabilities are within reach.

ANALYSIS OF ROLLING CONTACT STRESSES AND STRAINS

Crack intitiation, growth and fracture are closely related to the stresses and stress flucuations in the rim, particularly the shear stress fluctuations that accompany repeated rolling contact. The fluctuations arise as the contact approaches, passes directly over, and then leaves behind a particular portion of the rim on successive contact cycles (see Fig. 1). The fluctuating stress state depends on the contact stress distribution (both the pressure and friction related surface shear traction) and the resistance to plastic deformation which affects the peak stress levels and the accumulation of plastic strain in the rim.

The stresses and stress fluctuations are well defined for a linear elastic material. In this case, the contact stress distribution and the stress field in the rim can be described for the 2-dimensional (plane-strain) problem[1] (Hertz, 1882, 1896; Beliaev, 1924; Radzimovsky, 1953) and for

[1]The elastic contact pressure distribution for frictionless rolling (see Figure 1) is: $p(x) = p_o[1-x^2/w^2]^{0.5}$ in the region $-w<x<+w$, where x is the distance from the center of the contact, and w the half contact width,

$$w = \{(4P)/\pi[((1-\nu_1^2)/E_1 + (1-\nu_2^2)/E_2)/(1/R_1+1/R_2)]\}^{0.5}$$

where E, ν, and R are the elastic modului, the Poissons' ratios and radii of the 2 cylinders, and P is the load per unit of line contact transmitted by the contact. The stress field is given by the following expressions:

$$\sigma_z/\nu = \sigma_x + \sigma_y = 2p_o Re[ie^{-\zeta}]; \qquad \sigma_y - \sigma_x + 2i\tau_{xy} =$$

$$p_o i(\cosh\zeta - \cosh\bar{\zeta})e^{-\zeta})/\sinh\zeta; \quad \text{and} \quad x + iy = w\cosh\zeta.$$

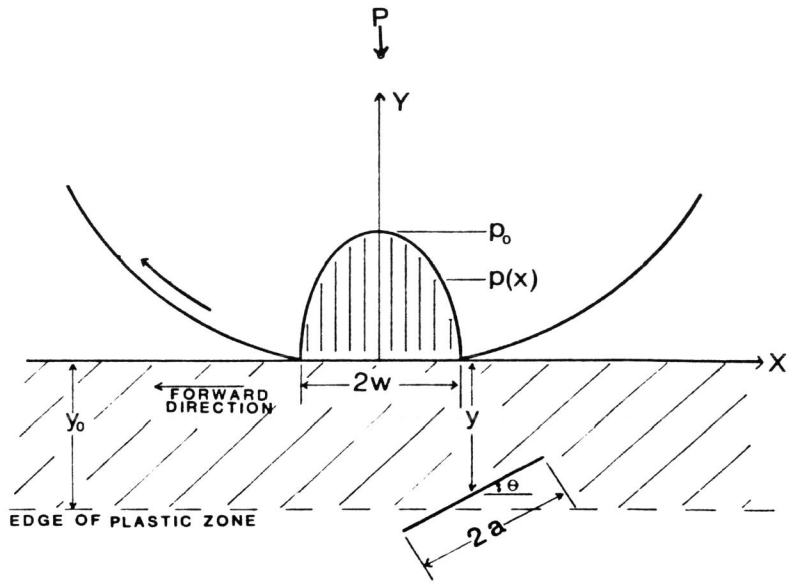

Figure 1. Schematic representations defining symbols used to describe the contact.

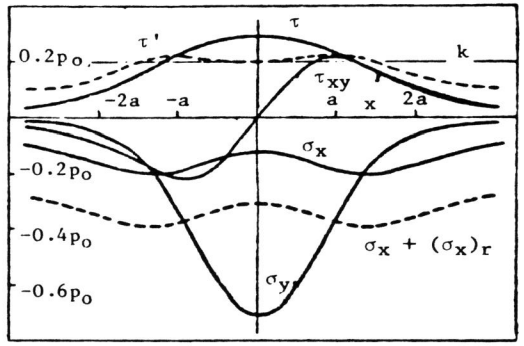

Figure 2. Variation of stress under the contact of the depth y = a as a function of contact position (Merwin and Johnson, 1963).

idealized 3-dimensional contacts (Kannel and Tevaarwek, 1981; Bryant and Keer, 1982). Merwin and Johnson (1963), and Johnson and Jeffris (1963) have devised an approximate treatment of the stress and strain states when the yield condition is exceeded for an elastic-perfectly plastic, strain amplitude independent von Mises material with a shear yield strength $k = \sigma_o/\sqrt{3}$ (σ_o is the uniaxial yield strength). Some of their results are compared with the elastic solution in Figure 2. The Merwin and Johnson (1963) treatment for frictionless rolling bounds 3 regimes of behavior in terms of the p_o/k-ratio (p_o is the peak contact pressure):

(i) Elastic behavior, $p_o/k < 3.1$. The material in the rim is subjected to purely elastic stress-strain fluctuations.

(ii) Transient elastic-plastic behavior or "shakedown", $3.1 < p_o/k < 4.0$. Elastic-plastic behavior in a shallow zone extending to a depth $y \approx w$ is reduced to elastic behavior in the first 3-5 contact cycles by the development of residual stresses.

(iii) Elastic-plastic behavior, $p_o/k > 4.0$. After 3-5 contacts, the material in the shallow, plastic zone experiences repeated, partially reversed, stress-strain cycles with small plastic strain amplitudes. This leads to the progressive accumulation of plastic strain -- "forward flow" -- in a layer extending to a depth $y \approx w$.

The p_o/k-bounds are influenced by the surface shear tractions produced when torque is transmitted by the rolling bodies. For example, the shakedown limit is reduced from $p_o/k = 4$ to $p_o/k = 1.85$, as the contact shear force-to-normal force ratio is increased from $T/P = 0$ to $T/P = 0.5$ (Johnson and Jeffris, 1963). Corresponding p_o/k-bounds for 3-dimensional contacts have not been derived.

Recent studies of an elastic-plastic finite element model of 2 dimensional rolling contact (Bhargava, Rubin and Hahn, 1984A, 1984B) confirm many features of the Merwin and Johnson (1963) analysis. For example, Fig. 3 clearly reveals the forward flow; Fig. 4 shows that steady state conditions of elastic-plastic behavior at $p_o/k = 5$ are obtained in the model material after 2 contacts. However, the calculations reveal that the material is subjected to stress-strain cycles with about 5 times larger plastic strain amplitudes than produced by Merwin and Johnson, i.e., $\Delta\varepsilon_{p,max} = 0.005$ at $p_o/k = 5$ (see Fig. 4), and that the stress-strain cycles are highly non-reversed (see Fig. 5). The implications of some of the unique features of the rolling contact stress field and stress strain cycles are listed below:

(i) Hydrostatic pressure. The contact field possesses a large hydrostatic component. For example, the mean pressure-to-yield strength ratio is in the range $0.89 < \sigma_m/\sigma_o < 2.89$ in the plastic zone directly below the contact for frictionless rolling at $p_o/k = 5$. Tensile stresses are only produced behind the contact when rolling is accompanied by relatively large surface shear tractions (Jahanmir and Suh, 1977). The hydrostatic pressure tends to close crack-like defects, causes the crack faces to rub, and precludes the opening, Mode I-type of crack loading.

(ii) Crack Driving Force. In the absence of large tensile stresses, the driving force for cyclic crack growth is predominantly Mode II in character and depends on the shear stress fluctuation resolved parallel to the crack plane.

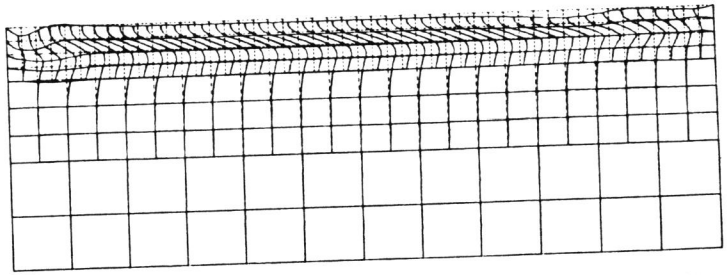

Figure 3. Elastic-plastic finite element model of rolling contact showing permanent deformation.

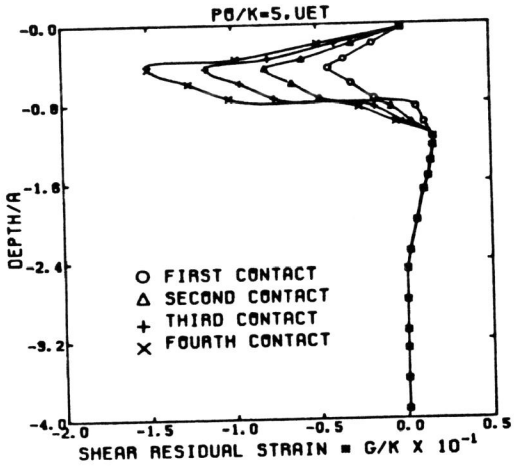

Figure 4. Elastic-plastic finite element calculation of the variation of residual strain with depth after successive rolling contacts (Bhargava, Rubin, and Hahn, 1984).

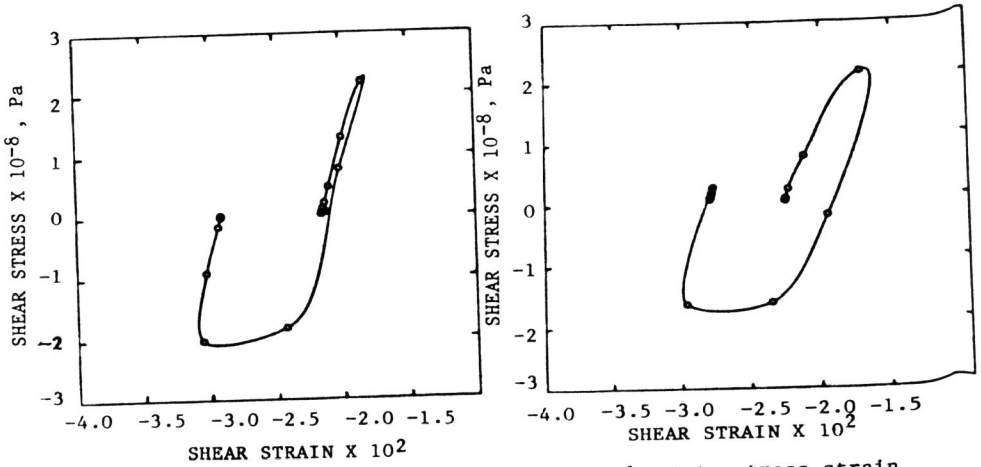

Figure 5. Finite element calculations of the steady state stress strain cycle at 2 locations in the rim at $p_o/k = 5$.

(iii) Cyclic Strain Hardening and Softening. The maximum value of the resolved shear stress fluctuation is limited by the resistance to plastic flow, $\Delta\tau_{max} = 2k$. The effective value of k will be elevated by cyclic strain hardening in regions of the rim experiencing the non-symmetric, large amplitude plastic strain cycles; the value of k will be reduced by cyclic softening in regions subjected to more symmetric, small amplitude cycles. The gradual elevation and lowering of k accompanying cycling will alter the character of the stress field and the strain cycles produced by successive contacts. For this reason, a steady state is not achieved until the values assumed by k at different depths saturate. This is consistant with observations which show that residual stresses continue to change after thousands of contacts (Fujita and Yoshida, 1977). It should be noted that the existing analyses of the contact stresses and strains all fail to account for cyclic hardening and softening.

(iv) Crack Face Friction. The friction acting at the faces of cracks closed by hydrostatic pressure will produce shear tractions that oppose the resolved shear stress and reduce the Mode II crack driving force (Rosenfield, 1980).

(v) Void Shrinkage. Plastic flow under the contact accompanied by a large hydrostatic pressure is expected to favor the shrinkage of voids and other open defects (Jahanmir and Suh, 1977). This may have a bearing on the likelihood of crack initiation in the plastic layer.

MEASUREMENTS OF CYCLIC HARDENING AND SOFTENING IN THE RIM

Measurements of the completely reversed cyclic flow properties of a number of materials are summarized in Fig. 6. These suggest that material subjected to peak cyclic strain amplitudes, $0.001 \leq \Delta\varepsilon_p \leq 0.01$, may harden, while material subjected to small plastic strain amplitudes farther from the rim may soften. The actual response of structural materials to the peculiar non-reversed cycles produced by rolling contact (Fig. 5) has not been examined. Microhardness traverses below the rim (on the x-y plane), of the type reproduced in Fig. 7, show substantial increases in hardness depths $2w < y < 4w$. The interpretation of these hardness increases is not straightforward, since the hardness impressions do not produce the same dislocation movements as the small amplitude strain cycles. However, there is no doubt that a change of hardness is a sure sign that plastic deformation has occurred during rolling. For this reason the hardness profiles in Fig. 7 show that plastic deformation has occurred at depths 2 times to 4 times greater than the depth of the plastic zone consistant with the value of k for monotonic loading, $y \simeq w$. This is a sign that the value of k appropriate for the largest depths and smallest amplitude cycles has been reduced by cyclic softening.

Further evidence of cyclic hardening and softening of the rim can be deduced from movement of wire markers implanted in the rim (Hamilton, 1963). The movement of the markers is a consequence of the non-reversed strain cycle which leads to the accumulating "forward" displacement of the rim visible in Fig. 3. The per contact amount of forward displacement at the surface is a function of k^{-1} (Merwin and Johnson, 1963 Hamilton, 1963). Consequently, the marker movements in Fig. 8 can be interpreted as follows:

- Markers in the rim of AISI 4140 steel (Fig. 8a) show significant forward flow at $p_o/k = 3.86$, where k is the monotonic shear resistance. This implies that the effective value of k is smaller than the monotonic value (e.g., cyclic softening) because the minimum value capable of

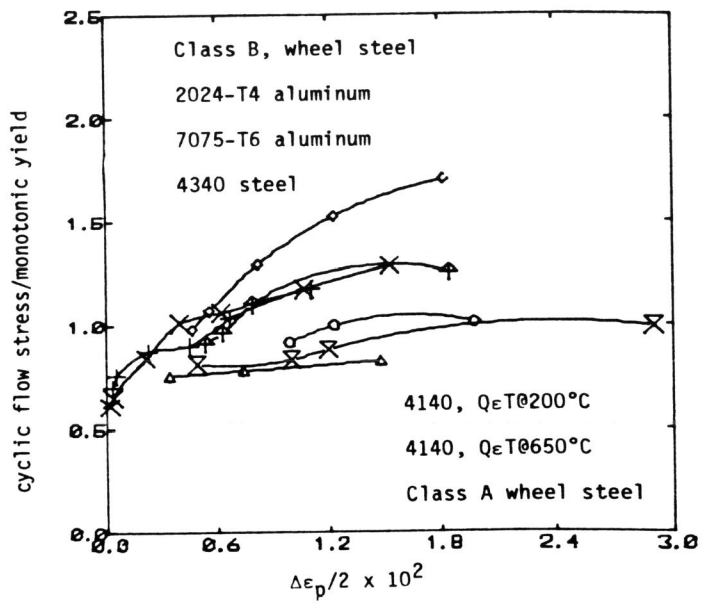

Figure 6. Variation of the cyclic flow stress with cyclic plastic strain amplitudes for fully reversed cycles and N = 50 cycles (Endo and Morrow, 1969; Thielen and Fine, 1976, and Stone and Dark, 1980).

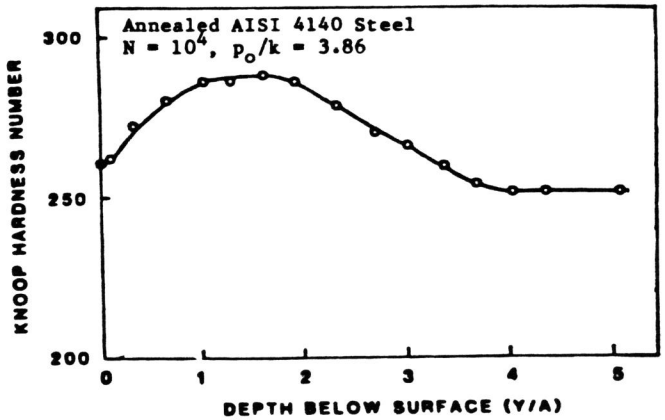

Figure 7. Variation of the hardness of the rim of a 50 mm-diadisk after $N = 10^4$ rolling contacts at $p_o/k = 3.86$ (Asuamah, 1982).

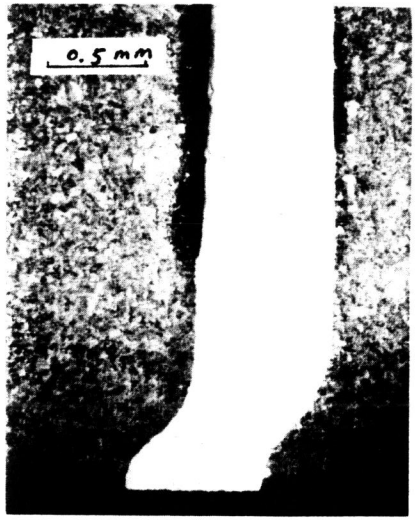

a. AISI 4140, $p_o/k = 3.86$
$N = 10^5$, a = 0.40 mm, B = 8mm

b. AISI 1018, $p_o/k = 7$, $N = 10^4$,
a = 0.19 mm, B = 12.5 mm

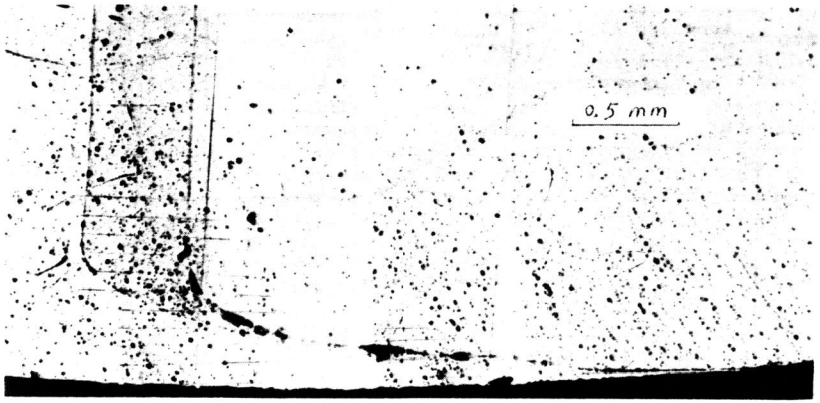

c. 1100 Al, $p_o/k = 6$, $N = 10^4$, a = 0.11 mm, b = 12.5 mm

Figure 8. Forward flow revealed by wire markers inserted in the rims of 50 mm diameter cylinders subjected to pure rolling.

producing forward flow (the shakedown limit) is $p_o/k = 4$.

• Markers in the AISI 1018 steel (Fig. 8b) show much less than 1/100 of the theoretically predicted forward displacement for $p_o/k = 7$. This can be viewed as a sign of strong cyclic hardening.

• Markers in the 1100 aluminum (Fig. 8c) display 2/3 of the theoretically predicted forward displacement. The absence of cyclic hardening in this case could be connected with the rapid recovery of cold work at room temperature.

MECHANISMS OF CRACK INITIATION

A number of workers have presented correlations between the cleanliness of steel and the life of bearings as illustrated in Fig. 9 (Hauser and Wells, 1970). Sugino, Miyamoto, and Nagumo (1971) have observed inclusions at spall origins, and Fregredo and Pritchard (1978) presented metallographic evidence of the conversion of inclusion particles into microcracks in rims with large amounts of forward flow. These studies show that inclusions are common crack intiation sites, but that the mechanisms involved are obscure. Jahanmir and Suh (1977) relate subsurface crack initiation produced by a rubbing asperity to the accumulation of a critical plastic strain. This idea is derived from analyses and experiments that connect particle decohesion or rupture with a critical tensile stress achieved after the onset of yielding (Argon, Im, and Safoglu, 1975; Argon and Im, 1975). However the large hydrostatic pressures make it virtually impossible to satisfy a tensile stress criterion in the case of frictionless rolling, unless the particles are either elastically very soft, already separated from the matrix, or involved voids. Evidence that voids located below the shallow plastic zone can nucleate cracks, is contained in Fig. 10. It appears that the nucleation process operating here is Stage I fatigue.

Other examples of crack initiation are visible in Figs. 11-13. Fig. 11 shows the condition of an 1100 aluminum wire marker installed in a 7075-T6 aluminum disk after $N = 10^4$ repeated rolling contacts at a $p_o/k = 4$. Several phenomena are evident. First, the wire marker has been forced deeper into the rim, and the cylinderical hole it occupied has been squeezed shut by the hydrostatic pressure. Secondly, some small cracks have initiated from the ends of the wire marker close to the rim. Finally, several long cracks have formed at a depth $y \approx 5w$, which is some distance below the plastic zone. Instances of crack intiation in a nickel wire marker close to the rim can be seen in Fig. 12a. Such a crack has completely severed a companion marker in Fig. 12b. In these cases the surrounding material has been forced into the void, and the crack has failed to penetrate the matrix. However, at a higher contact stress level, cracks in the wire extend into the matrix (see Fig. 13). These observations suggest that crack initiation at microstructural discontinuities is relatively easy but that it may be interfered with by the high hydrostatic pressure where yield conditions are satisfied. More work is needed to establish the nature of the "Stage I" crack intiation process, the size of the crack at the end of Stage I and a method for estimating the number of contacts required to intiate the crack.

DRIVING FORCE FOR CYCLIC CRACK GROWTH

The ΔK-driving force for cyclic crack growth depends on the size and geometry of the sub-surface crack, and on the contact stress distribution - -

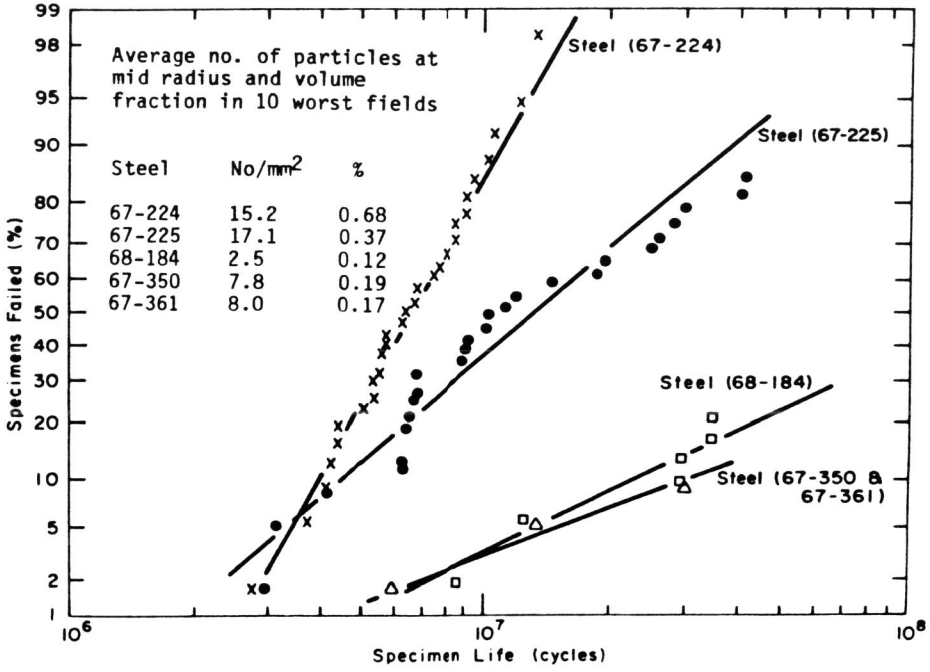

Figure 9. Weibull distribution curves for 52100 bearing steels showing effect of inclusion content on rolling contact rim life (Hauser and Wells, 1970).

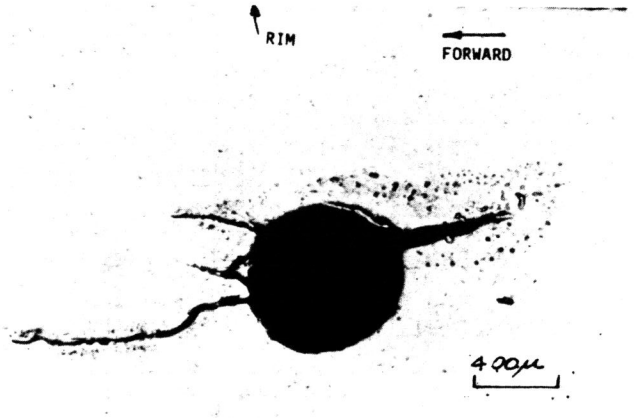

Figure 10. Cracks initiated at a 0.272 mm radius hole below the rim of 7075-T6 Aluminum subjected to N = 5 10^4 rolling contacts of p_o/k = 3.0 (Yoshimura, 1984).

Figure 11. Appearance of an 1100 Aluminum wire marker in the rim of a 50 mm, 7075-T6 aluminum disk after N - 10^4 rolling contacts at p_o/k = 4 (Huang and Hahn, 1983).

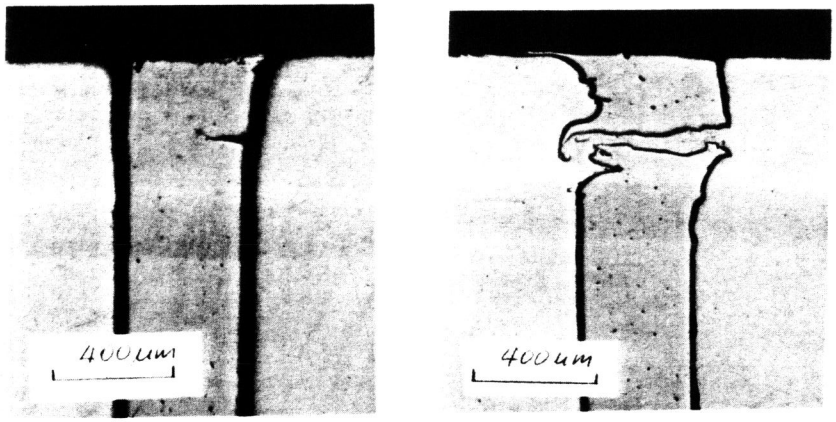

(a) (b)

Figure 12. Nickel-wire markers in the rim of 50 mm-diameter, 7075-T6 Aluminum disks subjected to $N = 1.1 \cdot 10^4$ contacts at $p_o/k = 3$ showing (a) crack nucleated in wire and (b) companion wire severed by crack with matrix material in wire cavity (Chiu and Hahn, 1983).

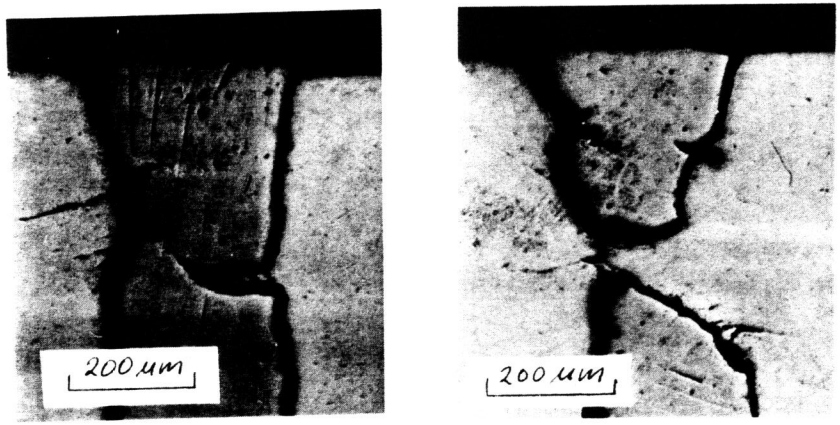

(a) (b)

Figure 13. Same a Figure 12 except disk subjected to N = 800 contacts at $p_o/k = 4$ showing: (a) severed wire marker and crack that has penetrated into matrix (arrow) and (b) aluminum matrix filled cavity and crack that formed and penetrated matrix before crack cavity was filled (Chiu and Hahn, 1983).

both the contact pressure and shear tractions. The opening mode (Mode I) of ΔK is absent when no torque is transmitted (frictionless rolling) since the contact normal stresses are everywhere compressive in this case. At the same time, the Mode II component, which produces relative sliding of the crack faces, is affected by the compression normal to the crack faces that creates a friction resistance to sliding. Consequently, both μ^R, the rim surface friction coefficient, and μ^C, the crack face friction coefficient enter the problem. A tabulation of friction coefficient values is given in Table 1. For relatively small surface shear tractions and μ^R-values, the character of the crack driving force is predominantly Mode II, but the ΔK_I and ΔK_{II}components are comparable in some cases (Hills and Ashelby, 1980). Figure 14 illustrates the variation of K_{II} with position of the contact relative to the crack. The crack face friction causes the crack faces to "stick" at certain intervals during which K_{II} is independent of position (the plateaus in Fig. 14).

A number of models of the physical problem that treat one or both sources of friction and different representations of the contact pressure have been evaluated. Hills and Ashelby (1980) treat a constant contact pressure and shear traction arising from the friction on the surface acting on a horizontal, subsurface crack in an elastic half-space without friction on the crack faces. Keer, Bryant and Maritos (1982) treat a cracked, elastic half-space loaded by a Hertzian contact pressure distribution and shear tractions consistant with the contact surface friction. They evaluate K_I- and K_{II}-values for both subsurface horizontal cracks and surface breaking, vertical cracks without friction on the crack faces. Keer and Bryant (1982) also treat the K_I- and K_{II}-values produced by a Hertzian pressure distribution with friction acting on an angled surface breaking crack. Keer and Bryant consider both friction on the crack faces and lubricant pressure in the crack cavity. In a more recent report, Hearle and Johnson (1983) derive values of K_{II} as a function of the relative contact position for horizontal subsurface cracks in an elastic half-space. In this case, the contact pressure distribution is approximated by a point force. Hearle and Johnson consider the friction at the crack faces as well as the friction on the contact surface and distinguish between the K_{II}-values produced at the leading and trailing ends of long cracks. O'Regan, Hahn and Rubin (1984) employ the contact stresses generated by Merwin and Johnson (1963) for an elastic-perfectly plastic rim subject to repeated, frictionless, rolling contacts. Results of this work, which evaluates the normalized driving force, $\Delta K_{II}/(p_o\sqrt{a})$, for "small" cracks as a function of x/w (the relative depth), θ (the crack inclination), and μ^C, are summarized in Figs. 14-16.

It should be noted that the peak value of ΔK_{II} is limited by the value of k (in the absence of friction $\Delta K_{II,max} = 2\ K\sqrt{\pi a}$). Consequently, cyclic strain hardening and cyclic strain softening affect the maximum values which the crack driving force can attain.

CYCLIC CRACK GROWTH da/dN-ΔK_{II} RELATION

Predictions of the cyclic crack growth hinge on the driving force-growth rate (da/dN-ΔK_{II}) relation, which is a material property. A number of techniques for measuring the cyclic crack growth rate under predominantly Mode II conditions have been devised (Roberts and Kibler, 1971; Shieh, 1975; Jones and Chisholm, 1975; and Otsuka, Mori, Ohshima, and Tsuyama, 1981), but very few measurements of the da/dN-ΔK_{II} relation have been carried out. As a result, the opportunities for predicting rim life and

TABLE 1 Summary of Friction Coefficient Values

Materials in Contact	Pressure, MPa	μ	Reference
7075-T6-AISI 4140	(high)	0.4-0.6	Shey (1980)
Al-4% Cu-steel	---	0.84-1.42	Linaud Wilmon (1969)
Al-1.8% Si-steel	0.6	0.5	Sarkar and Clarke (1980)
Al-6.3% Si-steel		0.34	
Al-13% Si-steel		0.48-0.64	
Al-4% Mg-0.7% Mn-steel	112	0.56-0.90	Wharton et al. (1973)
Aluminum (99.99%)-steel	~ 900	0.22	Peterson and Ling (1966)
	> 130	0.90-0.70	
Zinc (99.99%)-steel	~ 2000	0.22	
	~ 50	0.67	
Nickel (99.99%)-steel	~ 1240	0.32	
	~ 57	0.55	
Silver (99.99%)-steel	~ 1700	0.20	
	~ 56	0.40	
Indium (99.99%)-steel	~ 1150	0.05	
	~ 57	0.34	
Tin (99.99%)-steel	~ 1150	0.09	
	~ 57	0.28	
Cadmium (99.99%)-steel	~ 400	0.10	
	~ 57	0.21	
Ti-6%-Al-4%-steel	(high)	0.4-0.5	Shey (1980)
AISI 1018-AISI 1018	0.3	0.57	Ho, Noyan and Cohen (1983)
AISI 1020-AISI 1020	6.8	0.23-0.85	Mileston and Janeczko (1971)
	17.2	0.22-0.90	
AISI 1045-AISI-1045	0.141	0.6	Suhaud Sridhuran (1975)
AISI 4140-AISI-4140	(high)	0.7-0.8	Shey (1980)
AISI 4340-AISI 4340	0.7	0.58-0.81	Ho, Noyan and Cohen (1983)
Fe-0.39%C-5% Cr-(same)	---	0.26-0.79	Hogmark, Vingsho and Fridstrom (1975)
Fe-0.91%C-11.5% Cr-(same)	---	0.30-0.70	
Fe-1.50%C-11.5% Cr-(same)	---	0.19-0.82	

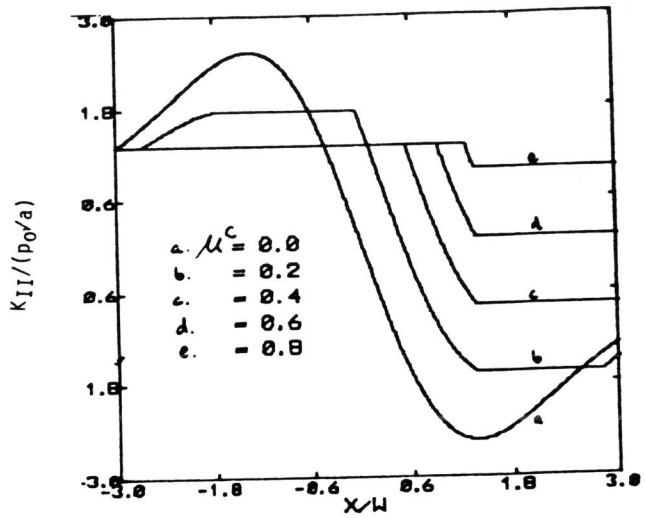

Figure 14. Variation of the K_{II}-stress intensity parameter with contact position for a subsurface crack: y/a = 1, θ =0, and p_o/k = 3 and different values of μ^c.

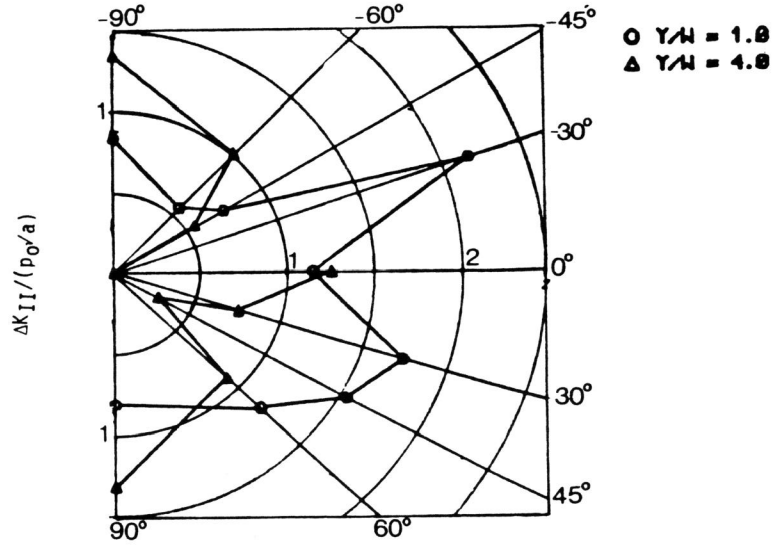

Figure 15. Variation of the ΔK_{II} driving force with crack inclination for subsurface cracks, and μ^c = 0.6.

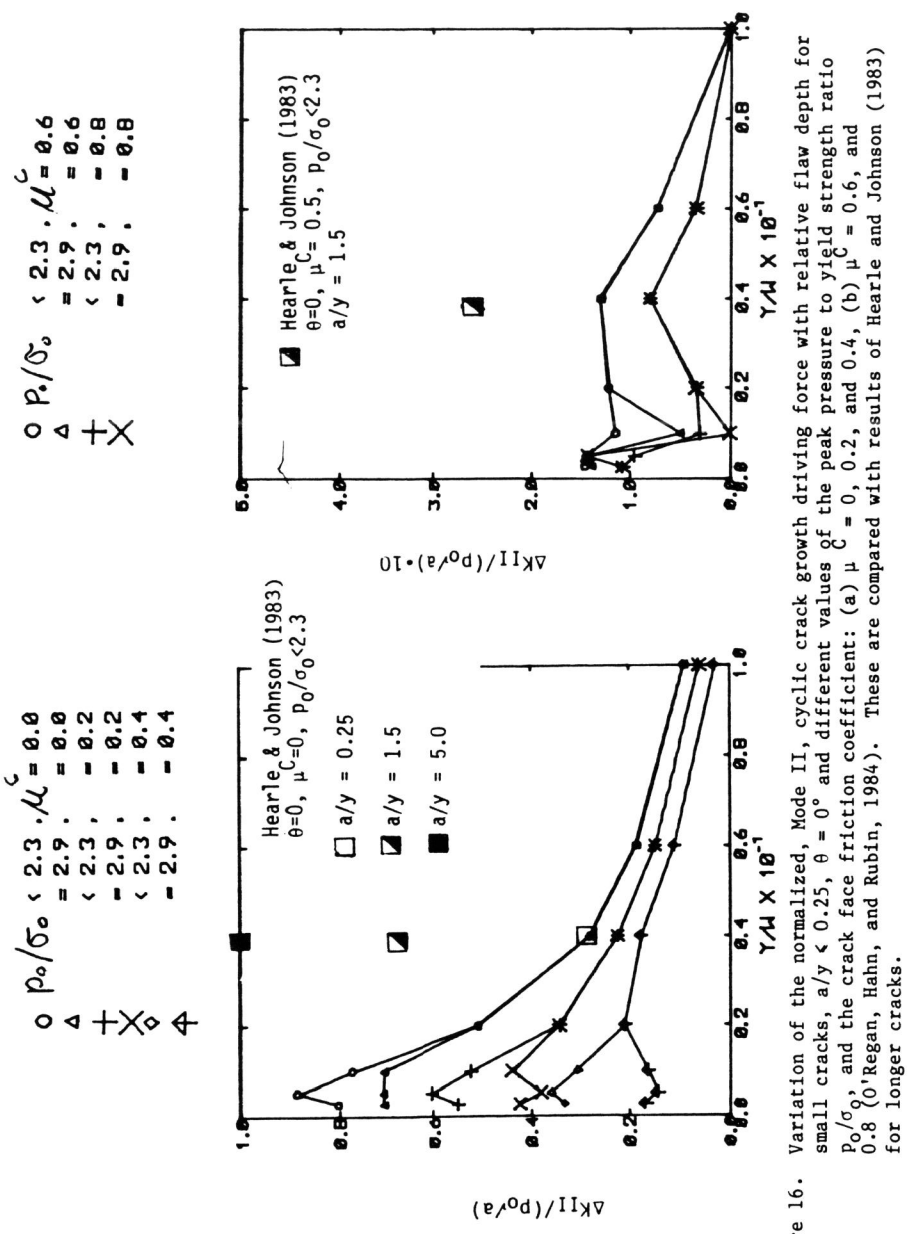

Figure 16. Variation of the normalized, Mode II, cyclic crack growth driving force with relative flaw depth for small cracks, a/y < 0.25, θ = 0° and different values of the peak pressure to yield strength ratio p_o/σ_o, and the crack face friction coefficient: (a) μ^C = 0, 0.2, and 0.4, (b) μ^C = 0.6, and 0.8 (O'Regan, Hahn, and Rubin, 1984). These are compared with results of Hearle and Johnson (1983) for longer cracks.

testing the reliability of such predictions are currently very limited.

Results reported by Otsuka, Mori, Ohshima and Tsuyama (1981) are reproduced in Fig. 17 and are employed in the next section.

APPLICATION OF FRACTURE MECHANICS TO RIM LIFE PREDICTION

In the absence of wear, the life of a rim is given by the number of contacts consumed by the crack initiation stage (when no pre-existing cracks are present) and by cyclic crack growth in the rim surface.

In principal, fracture mechanics methodology can quantify:

(i) the crack path
(ii) the number of contacts for cyclic crack growth from the initial (or intiation stage) size to the surface[2]
(iii) The initial flaw size that will assure a predetermined rim life, and
(iv) The "critical" flaw size, a*, below which cyclic crack growth does not occur.[3]

For example, an estimate of the "critical" flaw size for 7075-T6 aluminum (k = 275 MPa, $\Delta K_{II,Threshold} \approx 1$ MPa$\sqrt{m}$), for $p_o/k = 3$, $\mu^R = 0$, $\mu^C = 0.6$, derived with the aid of Figs. 15 and 16 (the maximum value of $\Delta K_{II}/p_o\sqrt{a} \approx 0.23$ for $\theta = -30^o$) is a* = 30 μm. The actual value is smaller for cracks close to the surface, i.e., a/y > 0.25, and could prove generally smaller since the estimate neglects departures from LEFM. This result reinforces the importance of cleanliness since a* approaches the size of large inclusion clusters.

A more direct test of the theory can be obtained from recent experiments in which a crack-like defect is installed below the rim of a disk and subjected to repeated rolling contact, as shown in Figs. 18 and 19 (Yoshimura, Rubin and Hahn, 1984). Table 2 compares the actual number of contacts ($N = 5.0 \cdot 10^4$) that produced measured amounts of crack growth with fracture mechanics predictions of N for likely bounding values of the crack face friction. While the agreement is encouraging, several features complicate the interpretation. For example, the calculations of the number of contacts in Table 2 do not take into account the branching and waviness of the crack profile evident in Figure 19b. The waviness combined with the compression could "key" the crack and substantially reduce its effective length. In addition, the larger ΔK_{II} driving force values for longer cracks reported by Hearle and Johnson (1983) and illustrated in Fig. 16 were not employed. The calculations summarized in Table 2 also illustrate that the number of contacts is very sensitive to the crack face friction which is difficult to evaluate for the conditions of interest. Figure 19 shows the crack profile on the midsection of the disk and on the surface after N = contacts. It appears that cracks grow more rapidly near the surface, possibly assisted by a Mode III component. This may be related to conclusions reached by Martin and Hay (1972) on the importance of

---

[2] $N = [An(Bp_o)^m]^{-1}[a_1^{-n} - a_2^{-n}]$, where A and m are empirical constants in the $da/dN = A\Delta K_{II}^m$ relation, $n = 0.5m - 1$, $\Delta K_{II}/(p_o\sqrt{a}) = B$, and B is a function of p_o/k, y/W, θ, μ^C and μ^R. This expression is valid for for small values of a when B is not a function of a.

[3] $a^* = [\Delta K_{II,Threshold}/(Bp_o)]^2$

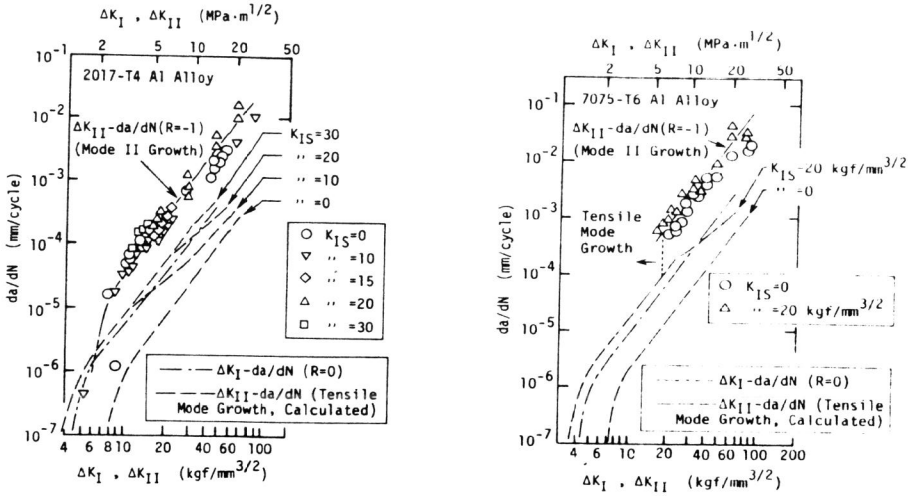

Figure 17. Measurements of the Mode II, ΔK_{II}-driving force for cyclic crack growth in 2017-T4 and 7075-T6 aluminum alloys (Otsuka, Mori, Ohshima and Tsuyama, 1981).

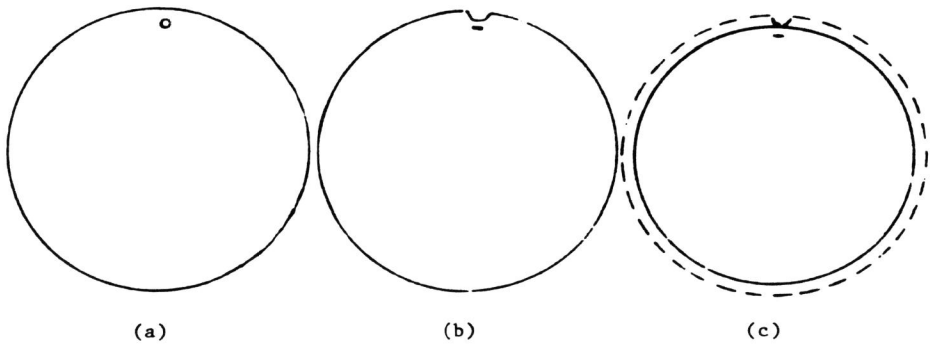

Figure 18. Procedure for inserting a crack-like defect below the rim of a rolling contact specimen: (a) drill small hole through disc, (b) indent rim collapsing hole, (c) remove indent by machining and heat treat specimen. (Yoshimura, Rubin and Hahn, 1984).

Figure 19. Profiles of surface cracks in a 50 mm diameter 7075-T6 aluminum test cylinder after rolling contacts at $p_o/k = 3.5$: (a) N = 0, midsection, (b) N = $2 \cdot 10^4$, midsection, and (c) N = $2 \cdot 10^4$, surface.

lateral forces on the propensity for the shelling of rails. Clearly, more experiments of the type summarized in Table 2 and more detailed analysis must be carried out before reliable predictions can be made.

TABLE 2 Comparison of Experimental Measurements of Subsurface Cyclic Crack Growth of Implanted Cracks in 7075-T6 Aluminum Disks Subjected to Repeated Rolling Contact with Fracture Mechanics Calculations*(Yoshimura, Rubin and Hahn, 1984; Yoshimura, 1984)

Experimental Conditions				N, Number of Rolling contacts		
p_o/k	y/W	a_1(mm)	a_2(mm)	Actual	Predicted	
					$\mu^C = 0.6$	$\mu^C = 0.8$
2.4	1.27	0.275	0.375	5.0×10^4	1.1×10^4	5.9×10^5
2.4	2.84	0.275	0.305	5.0×10^4	3.1×10^3	4.2×10^4
3.0	1.25	0.275	0.576	5.0×10^4	1.3×10^4	6.5×10^5
3.0	2.57	0.275	0.614	5.0×10^4	1.1×10^4	2.1×10^5

(1) $da/dN = A\Delta K_{II}^3$, $A = 3.36\cdot10^{-9}(MPa^3/m)^{-1}$(Otsuka, Mori, T. Ohshima and Tsuyama, (1981)
a_1 - intitial crack length
a_2 - final crack length

CONCLUSIONS

1. Existing analyses of the contact stresses and strains treat 2- and 3-dimensional contacts of elastic materials, and 2-dimensional (plane strain) contacts of elastic-perfectly plastic materials. None of thse analyses account for the cycle and plastic-strain-amplitude-dependent hardening and softening produced by repeated contacts.

2. The contact stress-strain field is characterized by a large hydrostatic pressure, and for $p_o/k > 4$, non reversed, small amplitude plastic strain cycles that produce an accumulating forward flow in a shallow plastic zone extending to a depth comparable to the contact width.

3. There is evidence that the plastic strain cycles produce a gradual cyclic hardening and softening with repeated contacts. A steady state may not be achieved for thousands of contacts until the values which k assumes at different depths saturate.

4. In the absence of wear, rim life is limited by the initiation and cyclic growth of subsurface cracks. Initiation proceeds at inclusions and voids, probably by a Stage I fatigue process. The high hydrostatic pressure may interfere with crack initiation.

5. Within the field of compression under the contact, the shear stress

fluctuations which produce relative sliding of the crack faces are the source of the predominantly Mode II, ΔK-driving force for cyclic crack growth. The compression normal to the crack faces creates a frictional resistance to sliding that reduces ΔK_{II}. Both the rim surface and crack face friction coefficients enter the problem. The ΔK_{II}-driving force produced by rolling contact conditions has been evaluated for a limited number of crack configurations and rolling conditions.

6. A number of methods of measuring da/dN-ΔK_{II} relations have been devised, but very few materials have been characterized so far.

7. A critical test shows that fracture mechanics predictions of cyclic crack growth attending frictionless rolling of 7075-T6 aluminum are in accord with a direct measurement.

8. In principle, the fracture mechanics methodology can quantify: (i) the crack path, (ii) the number of contacts for cyclic growth from the initial (or initiation stage) size to failure, (iii) the initial crack size that will assure a given rim life, and (iv) the "critical" size below which rim life is not limited by fatigue and fracture. In practice, the application of the methodology is still very limited because in the initiation stage, initial crack sizes and the relevant da/dN-ΔK_{II} relations and friction coefficients are inadequately defined.

ACKNOWLEDGEMENTS

This material is based upon work supported by the National Science Foundation under Grant No. DMR-8108500. The authors wish to thank Ms. Huang and Mr. A. Chiu for their contributions to the marker studies and Ms. C. Wieger for her work on the manuscript.

REFERENCES

Argon, A. S., J. Im, and R. Safoglu (1975). Met.Trans., 6A, 825-838.
Argon, A. S. and J. Im (1975). Met. Trans., 6A, 838-
Azuamah, C. O. (1982). M.S. Disseration, Vanderbilt University.
Beliaev, N. M. (1924). Eng'g. Construction and Structural Mech., Leningrad, 27-108.
Bhargava, V., G. T. Hahn, and C. A. Rubin (1984A). J. App. Mechanics, (to be published).
Bhargava, V., G. T. Hahn, and C. A. Rubin (1984B). Submitted to J. App. Mechanics.
Bryant, M. D. and L. M. Keer (1982). J. App. Mech., 49, 345-352.
Chiu, A. and G. T. Hahn (1983). Unpublished research.
Endo, T., and JoDean Morrow (1969). J. Materials, JMLSA, Vol. 4, No. 1, pp. 159-175.
Fegredo, D. M. and C. Pritchard (1978). Wear, 49, 67-78.
Fujita, K. and A. Yoshida (1977). Wear, 48, 301.
Hamilton, G. M. (1963). Proc. Inst. Mech. Engrs., 177, 667-675.
Hauser, J. J. and M. G. H. Wells (1970). AFML-TR-69-339.
Hearle, A. D. and K. L. Johnson, private communication.
Hengel, M. F. (1978). Proc. Sixth Int. Wheelset Congress, p. 3-31.
Hertz, H. (1882). Reine u. Angewandte Math., 92, 156-171.
Hertz, H. (1896). The Contact of Elastic Solids, Macmillan (London), 146-162.
Hills, D. A. and D. W. Ashelby (1980). Eng. Fracture Mech., 13, 69-78.
Ho, J. W., C. Noyan, and J. B. Cohen (1983). Wear, 84, 183-202.
Hogmark, S., O. Vingsbo, and S. Fridström (1975). Wear, 31, 39-61.

Hoo, J. C. (1982). Rolling Contact Fatigue Testing of Bearing Steels, ASTM STP 771.
Huang, J. and G. T. Hahn (1983). Unpublished research.
Jahanmir, S. and N. P. Suh (1977). Wear, 4, 17-38.
Johnson, K. L. and J. A. Jefferis (1963). Proc. Symp. Fatigue in Rolling Contact,Inst. of Mech. Engr., London, p. 5.
Jones, D. L. and D. B. Chisholm, Engg. Fracture Mech., 7, 261-276.
Kannel, J. W. and J. L. Tevaarwerk (1981). NASA CR-165561, 1-31.
Keer, L. M., M. D. Bryant, and G. K. Haritos (1982). J. Lubrication Tech., ASME, 104.
Keer, L. M. and M. D. Bryant (1982). J. Lubrication Tech., ASME, 82-Lub-10.
Kunikake, T., S. Nishimura, and H. Tagashira (1970). Trans. ISIJ, 10, 476-489.
Lin, D. S. and H. Wilman (1969). Wear, 14, 323-335.
Lundberg, G. and A. Palmgren (1947). Ing. Vetanskap, Akad.-Handl, No. 96.
Martin, G. C., and W. W. Hay (1972). Trans. ASME, 72-WA/RT8.
Merwin, J. E. and K. L. Johnson (1963). Proc. Inst. Mech. Engrs., 177, 676-685.
Milestone, W. D. and J. T. Janeczko (1971). Wear, 18, 29-40.
O'Regan, S., G. T. Hahn, and C. A. Rubin, (1984). To be published.
Otsuka, A., K. Mori, T. Ohshima, and S. Tsuyama (1981). Advances in Fracture Research, Vol. 4, Pergamon Press, 1851.
Peterson, M. P. and F. F. Ling (1966). Friction and Lubrication in Metal Processing, ASME, 39-67.
Radzimovski, E. I., (1953). University of Illinois Exp. Sta. Bulletin No. 408.
Roberts, R. and J. J. Kibler (1971). J. Basic Engg. ASME, 93, 671-680.
Rosenfield, A. R. (1980). Wear, 61, 125-132.
Sarker, A. D. and J. Clarke (1980). Wear, 61, 157-167.
Schey, J. A. (1980). Journal of Metals, 32, 28-33.
Shieh, W. T. (1977). Engg. Fracture Mech., 9, 37-54.
Stone, D. H., and Y. J. Park (1980). ASME App. Mech. Div., Vol. 40, p. 157.
Sugino, K., K. Miyamoto, and M. Nagumo (1971). Trans. ISIJ, 11, 9-17.
Suh, N. P. and P. Sridharan (1975). Wear, 34, 291-299.
Syniuta, W. D., and C. J. Corrow (1970). Wear, 15, 187-199.
Thielen, P. N., Fine, M. E. and R. a. Fournelle (1976). Acta Metallurgica, Vol. 24, 1-10.
Wharton, M. H., R. B. Waterhouse, K. Hirakawa, and K. Nishioka (1973). Wear, 26, 253-260.
Yoshimura, H., C. A. Rubin, and G. T. Hahn (1984). Wear (to be published).